JOURNAL OF MATERIALS SCIENCE **34** (1999) 2911–2920

Rapid oxidation of liquid tin and its alloys at 600 to 800 °C

D.-W. YUAN*, R.-F. YAN, G. SIMKOVICH
Department of Materials Science and Engineering, Pennsylvania State University, University Park, Pennsylvania 16802, USA
E-mail: yuan@ctc.com

The behavior of liquid tin and its alloys in oxygen at temperature range 600 to 800 °C were investigated. Rapid and nearly linear reaction kinetics were observed for pure tin at temperature higher than 700 °C. Marker experiments, which determine the mode of mass transport through the scale, and wetting phenomena between the oxide and melts were studied to delineate the reaction mechanism of oxide growth. Moreover, the rates of oxidation of tin were markedly changed by alloying it with small amount of foreign elements. Significantly increased oxidation rates for binary tin alloys containing Mg, Ba, La or Ca were observed. TEM studies indicated that additional growth stresses were introduced into the SnO_2 scales by these additions.

1. Introduction

Rapid oxidation of liquid metals and alloys is considered to be detrimental because it results in excess material losses and alloy compositional changes. Special processing practices, such as controlled atmospheres and reduced ambient pressures, have been commonly employed to curtail the oxidation rate. Nevertheless, exceptionally rapid reaction kinetics of the melts has exhibited the ability to form unconventional composite structure. Newkirk *et al.* [1, 2] first reported the formation of Al_2O_3/Al ceramic composite materials when appropriate minor alloying elements were added to superheated Al melts. This processing technique, commonly known as the DIMOX^{TM} directed metal oxidation process [3], only reaches its potential when stringent processing conditions are met. Similar reaction behavior has since been identified to form AlN/Al and ZnO/Zn type materials by carefully selecting the alloy composition and the reaction temperature [4–6].

It is clear that oxidation behavior of liquid metals at temperatures significantly higher than their melting points has been of little interest to researchers in the past. However, unique characteristics of the DIMOX^{TM} process provide incentives to reexamine the reaction kinetics of melts in oxidizing environments. In this study, tin was chosen as the parent metal because of its low melting point (232 °C) and moderate oxidation rates in the liquid state. Most of the previous investigations in the gaseous oxidation of tin and its alloys have been limited to temperatures below 500 °C [7–9]. Focus of the efforts is, therefore, directed to determine the rates of oxidation at 600, 700 and 800 °C. Also, little is known about the impact of minor alloying elements on the oxidation kinetics of melts at these temperatures. Kinetic studies are conducted on liquid tin with the additions of elements of different oxygen affinity. Furthermore, oxidation mechanisms, which account for the rapid kinetics observed, are to be deduced.

2. Experimental

The alloys used in this investigation were made by melting charges of 99.99% pure tin with chemically pure grade alloying elements. The metals were assembled according to the stoichiometry chosen, in atomic percent (at %), and placed in Al_2O_3 crucibles. The crucibles were then encapsulated in Pyrex glass tubing which had been evacuated and backfilled with argon to prevent oxidation. All the thermal treatments were performed in a muffle furnace. When the parent metals became entirely molten and the alloying constituents had completely dissolved, the capsules were then shaken periodically to ensure complete mixing. The melts were allowed to furnace cool to attain nearly planar surfaces.

Kinetics measurements were made in pure oxygen or in oxygen atmospheres diluted with argon via thermogravimetric analysis (TGA). Both weight gain per reaction area (mg/cm^2) and the corresponding relative weight gain (%), which is characterized by the ratio of the gain in weight of the content in the crucible to the theoretical weight gain for complete conversion of metal to ceramic phase, were monitored. In the calculation, SnO_2 is considered as the only stable oxide formed at the reaction temperatures. The nominal cross-sectional area of the Al_2O_3 crucibles, 2.1 cm^2, was used as the material growth surface area for the calculation of reaction rates. Short time oxidation tests were also performed to study microstructural developments as a function of time and temperature.

* *Present address*: Concurrent Technologies Corporation, Johnstown, PA 15904, USA.

Optical microscopy was used to characterize the result ing reaction products. Volume fractions of the phases were determined from photographs by point-counting techniques. Debye-Scherrer powder X-ray diffraction techniques were used to identify the phases in thin oxide scales. The patterns were obtained using Ni-filtered Cu$K\alpha$ radiation. A Scintag powder X-ray diffractometer (XRD) was also employed for the phase identification of bulk materials. In addition, the reaction products of Sn alloys were examined by a Phillips 420T transmission electron microscopy (TEM) operating at 120 kV.

Marker experiments were performed in which inert, fine alumina particles were placed on the surface of pure tin. Alumina was chosen because the oxygen affinity of aluminum is higher than that of tin and very small solid solubility is likely. The specimen was oxidized for 10 min at 700 °C in pure oxygen and then metallographically examined. The wetting behavior of the alloy melts on tin oxide was also investigated to determine if liquid alloys could infiltrate into the porous oxide body by a capillary effect. Wetting experiments were carried out in a horizontal tube furnace fitted with an observation window through which one could photograph a sessile drop. The samples were assembled and outgassed in the furnace with cleansed argon for 4 h before heating.

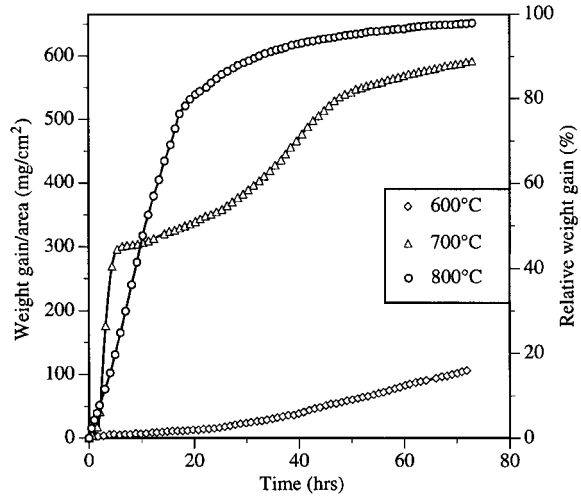

Figure 1 Weight changes for pure tin at 600, 700 and 800 °C, respectively, in 1 atm O_2.

3. Results and discussion

3.1. Pure Tin

The oxidation kinetics of liquid pure tin at temperature ranging from 600 to 800 °C are illustrated in Fig. 1. A distinct increase in the oxidation rate occurs when temperature is increased from 600 to 700 °C. Upon increasing the temperature to 800 °C, a nearly linear rate is sustained up to 16 h. After 72 h in O_2 at 800 °C, more than 97% of the metal has been reacted to form oxide. The appearances of the final reaction products vary considerably at different temperatures. At 600 °C an uneven and crazed surface is observed. In contrast, a few columnar protrusions start to grow outward from the original reaction surface at 700 °C. When tin is oxidized at 800 °C, the protrusions become longer and thicker and often dumbbell-shaped oxide bodies are formed. Similar outward growth of the reaction products is also observed when other crucible material, such as fire clay, is used. For pure tin with an oxide volume/metal volume ratio of 1.31, one would expect compressive stresses in the oxide layers. Initially, the oxide scales may deform and maintain contact between the metal and the scale when they are thin. But, as the scales grow in thickness, they become increasingly difficult to deform, and defects may be formed in the scale. Therefore, continued oxidation causes a build-up of stresses in the scale/metal system and eventually the scales fracture. As a result, it leads to more metal exposed to the oxygen, and breakaway oxidation occurs.

To better examine the microstructural evolution, short time experiments were performed for intermediate reaction times. Fig. 2 shows an optical micrograph

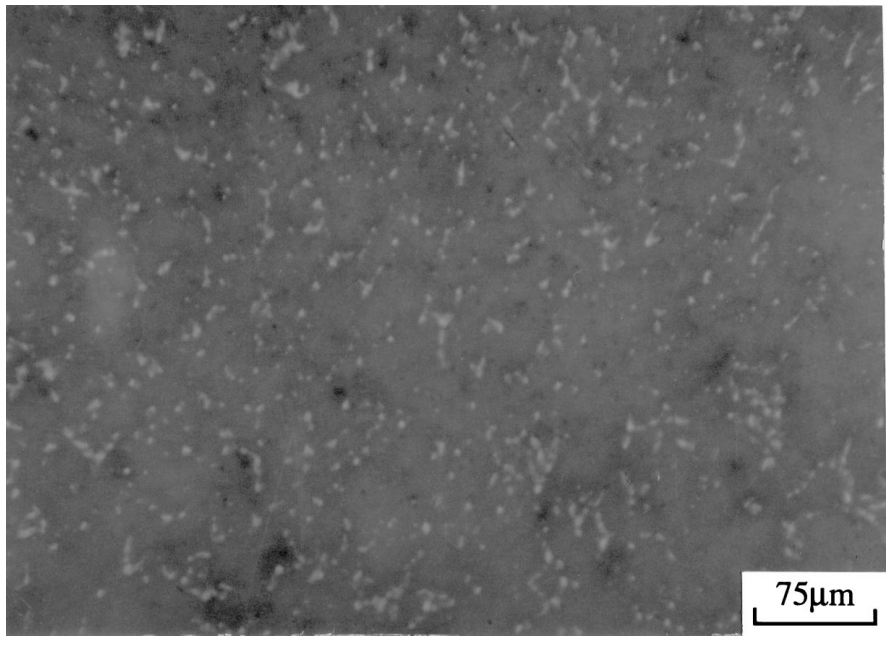

Figure 2 Optical micrograph of the reaction product of pure Sn Oxidized at 800 °C for 6 h.

of the cross-section of the reaction product, which is removed from the furnace after soaking at 800 °C for 6 h. It consists of fine second phase particles in a predominant matrix. The volume percentage of the second phase in the material is ∼12%. Powder X-ray diffraction data for the bulk materials identifies that SnO_2 is the matrix phase and metallic tin is the minor one. For longer reaction times at 800 °C, the amounts of tin in the resultant materials decrease and porosity is observed in the matrix.

3.2. Binary tin alloys

It is known that various factors, particularly thermodynamics and kinetics, determine the overall scale development. In other words, the relative Gibbs energies of formation of the oxides can be used to predict which is the thermodynamically favored oxide. However, they do not determine completely the nature of the transient oxide or of the steady state scale. For tin based alloys, the dopants used have been found to affect the oxidation reaction significantly [7]. To facilitate interpretation of the oxidation kinetics and the resulting microstructures, studies on the oxidation behavior of liquid tin alloys are limited to binary alloys which contain low concentrations of second elements. Fig. 3a shows the kinetic results for various tin binary alloys oxidized at 700 °C in pure oxygen. All the alloying elements used are less oxygen-reactive than tin. Therefore, Sn is expected to be preferentially oxidized initially. For the first 4 h, the oxidation rates of pure tin and those binary alloys are very close indicating the alloying elements do not actively participate in the reaction. As the reaction time increases, activities of the alloying additions in the melts gradually increase, which determine the subsequent oxidation behavior of the alloys.

Fig. 3b shows the TGA results for tin alloys containing elements of higher oxygen affinities than the parent metal at 700 °C. Zn and Ca are beneficial additive which significantly reduce the oxidation rate of the respective alloys; alloys containing Ba or Mg exhibit considerably faster rates. Those oxide scales responsible for the sluggish rates were examined more carefully to determine the causes. Energy-dispersive spectroscopic analyses show that Zn is the only metallic constituent in the oxide scale of a Sn-3Zn alloy, while both Ca and Sn are detected in the scale of the Sn-3Ca alloy. It has been demonstrated that a ZnO scale is compact and protective at the reaction temperature [6, 10]. Therefore, the preferentially formed ZnO layer on the reaction front shuts down the oxidation. In contrast, a CaO and SnO mixture is identified on the Ca-rich scale by the Debye-Scherrer X-ray data (Table I). Possible formation of a (Ca, Sn)O solid solution would increase the oxide volume to metal volume ratio of the scale and consequently makes it more compact and oxidation-resistant. On the other hand, the differences in size between Mg^{2+} and Sn^{2+} (23%) and between Ba^{2+} and Sn^{2+} (46%) are fairly large (Table II). This suggests that the formation of two separate scales at the initial stage of oxidation is more likely than the formation of (Mg, Sn)O or (Ba, Sn)O solid solution in the scale.

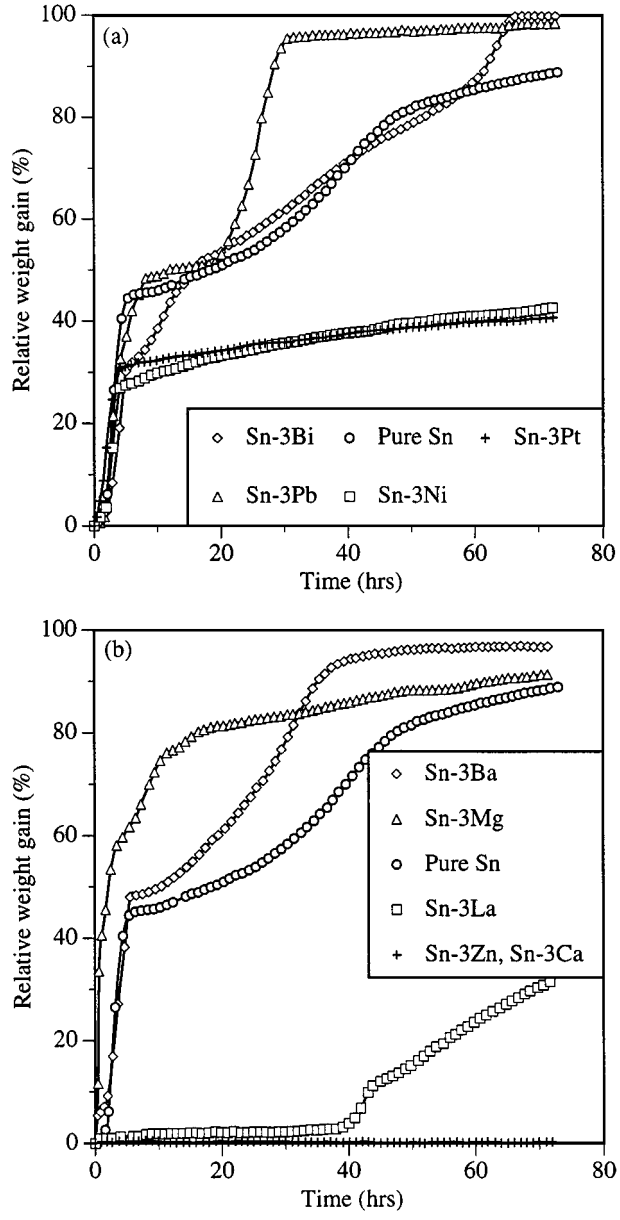

Figure 3 Weight changes for Sn alloys, containing alloying elements with (a) lower and (b) higher oxygen affinities, at 700 °C in 1 atm O_2.

Moreover, Aylmore *et al.* [11] found that MgO and BaO formed during the oxidation process possess very high specific surface areas. It can be assumed that the formation of porous MgO or BaO scales on the surface exposes more materials to the attack of oxygen, which results in faster rates of oxidation.

The oxide growth rates at 700 °C were further examined by varying the amounts of selected alloying elements. Fig. 4 shows the kinetics of Sn alloyed with different amounts of Mg (1, 3 and 6%) and Li (3 and 6%). For Sn-Mg alloys, low Mg concentration (1%) results in an initial reduction in oxidation rate; however, all three alloys attain close to 90% relative weight gain at the end of the experiments. For Sn-Li alloys, higher Li concentrations result in slight decreases in the amounts of metal converted to oxide. All these results indicate that the influence of dopant itself outweighs the influence of dopant concentration in determining the overall oxidation rates. Thus, the concentration of the alloying addition was fixed at 3 at %.

TABLE I Interplanar spacings and phases present for the oxide scale of Sn-Ca alloy

d_{obs} (Å)	I_{obs}	Sn (JCPD4-673)	SnO (JCPD24-1342)	CaO (JCPD37-1497)
2.911	100	2.915_X	2.90_8	
2.776	100	2.793_9	2.78_8	2.77_4
2.639	40		2.63_X	
2.394	40			2.406_X
2.253	30		2.24_1	
2.063	50	2.068_3		
2.011	80	2.017_7		
1.792	10		1.80_1	
1.759	10		1.75_2	
1.697	30			1.70_5
1.654	60	1.659_2	1.66_5	
1.586	20		1.572_5	
1.481	50	1.484_2		
1.455	60	1.458_1		1.451_2
1.439	40	1.442_2		
1.422	10		1.426_1	
1.388	10		1.382_2	1.389_2
1.326	40			1.33_3
1.301	30	1.304_2		
1.289	30	1.292_2		
1.202	40			1.202_1
1.093	30	1.095_1		1.104_1
1.075	10			1.076_2
1.043	30	1.043_1		
1.039	20	1.03_1		

TABLE II Ionic radii for selected elements

Element	Radius (Å)
Ba^{2+}	1.36
Bi^{3+}	0.74
Ca^{2+}	1.00
La^{3+}	1.06
Li^{+}	0.74
Mg^{2+}	0.72
Ni^{2+}	0.69
O^{2-}	1.40
Pb^{2+}	1.18
Sn^{2+}	0.93
Sn^{4+}	0.71
Zn^{2+}	0.75

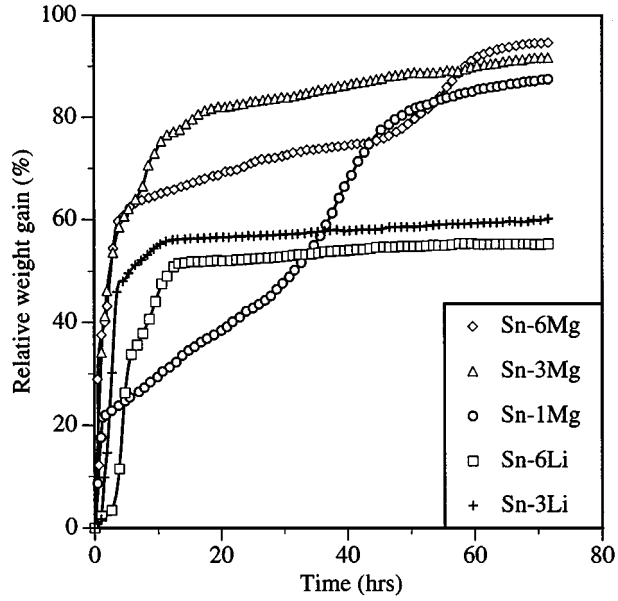

Figure 4 Weight changes for various Sn-Mg and Sn-Li alloys at 700 °C in 1 atm O_2.

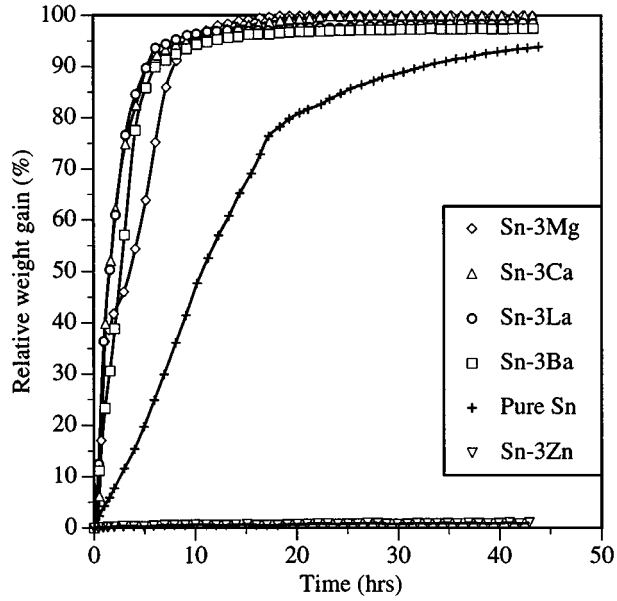

Figure 5 Weight changes for various binary Sn alloys at 800 °C in 1 atm O_2.

Oxidation behavior of tin alloys containing additives of higher oxygen affinities at 800 °C was further studied. The resulting growth rates of various alloys are shown in Fig. 5. The addition of Zn essentially terminates the oxidation, while significant increases in the oxide growth rates are observed for alloys containing low concentrations of Ba, Ca, La and Mg. Sluggish rates were previously observed for Ca and La containing alloys at 700 °C. The sharp contrast in kinetics between 700 and 800 °C could be caused in part by the increase in growth stress at higher temperature, which leads to fracture of protective scale. Examinations on the polished sections of the reaction products of binary alloys oxidized at 800 °C reveal microstructures similar to that shown in Fig. 2. It contains an oxide matrix and a tortuously shaped metallic phase. XRD analysis shows that the two constituents are SnO_2 and tin. No phases containing any of the alloy additions are identified.

3.3. Growth mechanism of tin oxide based materials

One of the typical characteristics of the DIMOX™ process is the observation of cavities at the bottom of the crucibles due to outward growth of the reaction products. Visual examinations on the cross-sections of the reaction products of tin-based alloys do not reveal the presence of such cavities. Though near constant growth rates are observed for tin and its alloy at elevated temperatures in oxygen, it is conceivable that the mechanism for the rapid growth of tin oxide is quite different from the one for the DIMOX™ type process.

Fig. 6 shows the surface morphology of a pure tin specimen after being oxidized at 800 °C for 10 min in 0.05 atm oxygen. The low oxygen partial pressure was employed to retard the oxide growth and therefore facilitated the study of the oxidation phenomena at an initial

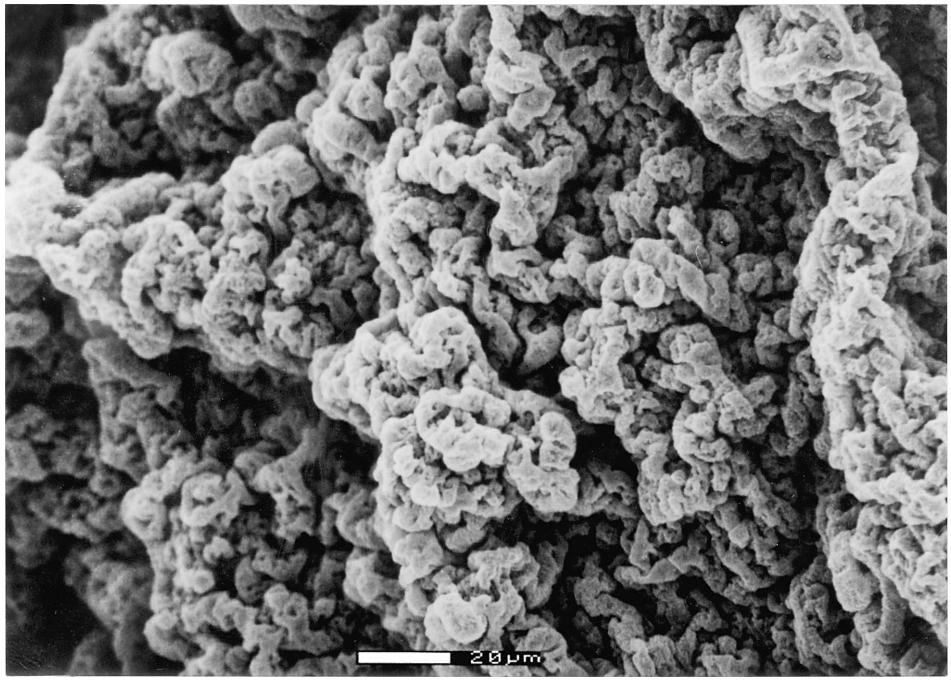

Figure 6 Surface morphology of pure tin after oxidizing at 800 °C for 10 min in 0.05 atm O_2.

stage. The porous surface topography shown suggests that the oxidation of liquid tin alloys proceeds via the passage of oxygen through the oxide scales. It follows that new oxide is formed at the oxide/metal interface. The cause for the formation of such porous scale could be in part attributed to the phase transition in the oxide formed. It is generally agreed that SnO, which forms at the initial stage of oxidation of tin, is metastable and decomposes according to the reaction [12]

$$2SnO = SnO_2 + Sn \tag{1}$$

Moreover, higher the reaction temperature faster is the rate of phase transformation from SnO to SnO_2.

Pure liquid tin is shown to oxidize rapidly especially at 700 and 800 °C. This can be rationalized by the relatively higher stability of SnO, which formed initially, at 600 °C but not at 700 and 800 °C. As might be expected, phase transition can change the plasticity of the oxide scale. Also, differences in crystal structure, ion and dislocation mobility in the two oxides produce mismatches in degree of compactness and protective ability of oxide scales. In addition, 5% increase in the atomic volume on going from SnO to SnO_2 can further build up stresses and lead to the breakdown of oxide scales. A delay in phase transformation at 600 °C suggests that less stress and fewer defects may be produced in the scale and, therefore, the oxidation rate of pure tin is reduced.

For binary Sn alloys, significant reductions in oxidation rates are obtained at 700 °C as a result of the transition delay by dissolution of CaO in SnO. At 800 °C, the ever-decreasing thermodynamic stability of SnO makes the transition inevitable and, consequently, the scales are no longer protective. Moreover, the development of a locally highly stressed region leads ultimately to blister-like crack formation. If the cracking of the new film occurs at different times at different sites over the specimen surface, the various "rate curves" for each such microscopic area must blend into a straight line, thus accounting for the linear portion of the macroscopic rate curve.

In the marker experiments, Fig. 7 presents a SEM micrograph of the cross section of oxide scale on metal substrate with the alumina particles visible. The markers neighbor the metal/scale phase boundary. This indicates that formation of the reaction products takes place due to the outward diffusion of metal atoms, and not as a result of inward diffusion of the oxidant. However, this finding does not agree with the current understanding of the defect chemistry of SnO_2. According to Wanger's theory [13], the mass transport through the scale is determined by the defect structure of the scale when diffusion of a particular reactant is involved in the overall process. If the reaction product consists of only anion defects, the scale growth can take place only as a result of inward diffusion of the oxidant species. In the case of SnO_2, oxygen vacancies are the predominant defect species in the defect structure according to Shuey [14].

$$SnO_2 = 2V_O^{\cdot\cdot} + 4e^{'} + Sn_{Sn}^{X} + O_2 \tag{2}$$

Therefore, inward diffusion of oxygen should prevail and leave the markers at the oxide/gas interface. Nevertheless, the disagreement can be understood based on two facts. First, the interpretation of the marker study is valid primarily for growth of dense scales. Thus, the formation of pores and cavities in the oxide scales, as discussed previously, could affect the marker locations. Second, the occurrence of SnO to SnO_2 phase transition in the oxidizing environment further complicates the interpretation. No systematic study has been done on the defect structure of SnO. Boggs *et al.* [15] suggested

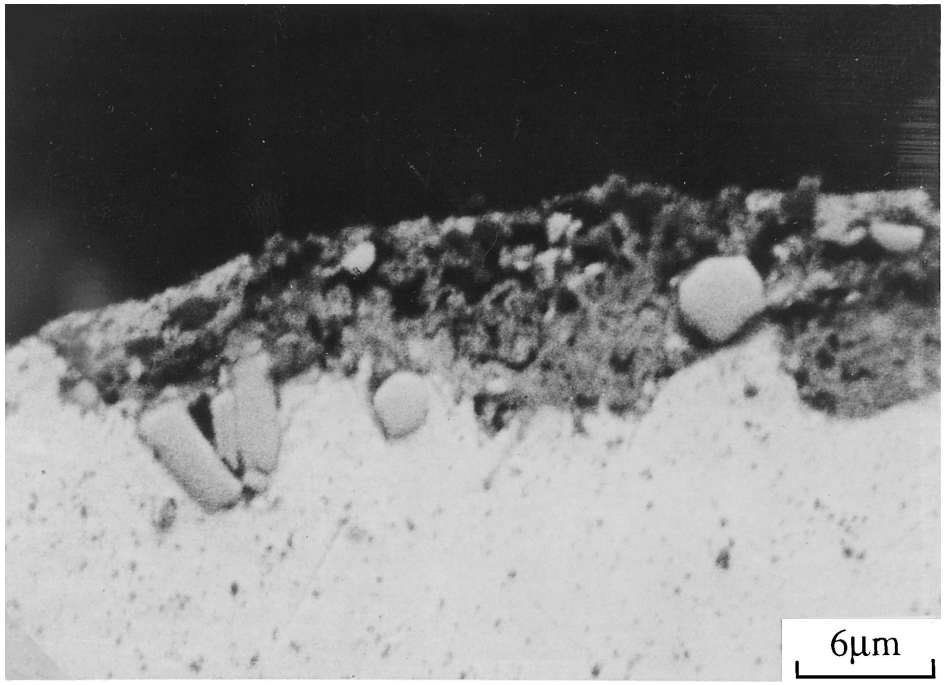

Figure 7 Cross-section of pure tin after oxidizing at 700 °C for 10 min (the particles at oxide/metal interface are the Al_2O_3 markers).

that SnO could be a p-type, cation-deficit semiconductor. Their conclusion was based on two observations: (1) the cavities found between the SnO film and the metal during oxidation was assumed to be caused by the movement of tin ions through a thickening oxide scale, and (2) the oxidation rate of a Sn alloy at low temperatures was in the direction predicted by Hauffe's valence rule [16]. Thus, the location of these Al_2O_3 marker in Fig. 7 can be fitted into the argument if a p-type metal deficit SnO scale is formed initially.

Fig. 8 shows the results of thermogravimetric measurements on pure tin at 800 °C as a function of oxygen partial pressure ranging from 0.03 to 1 atm. The linear growth rates at 800 °C are then found to be proportional to the oxygen pressure as shown in Fig. 9a. A similar oxygen activity dependence is observed for Sn-3Mg alloy (Fig. 9b). For an equilibrium reaction

$$\mathrm{Sn} + \mathrm{O_2} \underset{k_2}{\overset{k_1}{\Leftrightarrow}} \mathrm{SnO_2} \tag{3}$$

where k_1 and k_2 are the forward and backward rate constants, respectively. The oxidation rate $(\dot{n}/A)$ can be expressed as

$$(\dot{n}/A) = k_1 \cdot P_{\mathrm{O_2}} \cdot a_{\mathrm{Sn}} - k_2 \cdot a_{\mathrm{SnO_2}} \tag{4}$$

where a is the activity. If SnO_2 and Sn are almost pure, the activities of Sn and SnO_2 are equal to unity. Therefore, a linear relationship between the partial oxygen pressure and oxide growth rate can be expected based on Equation 4, assuming the backward reaction constant (k_2) may be neglected. The experimental results are in good agreement with the prediction.

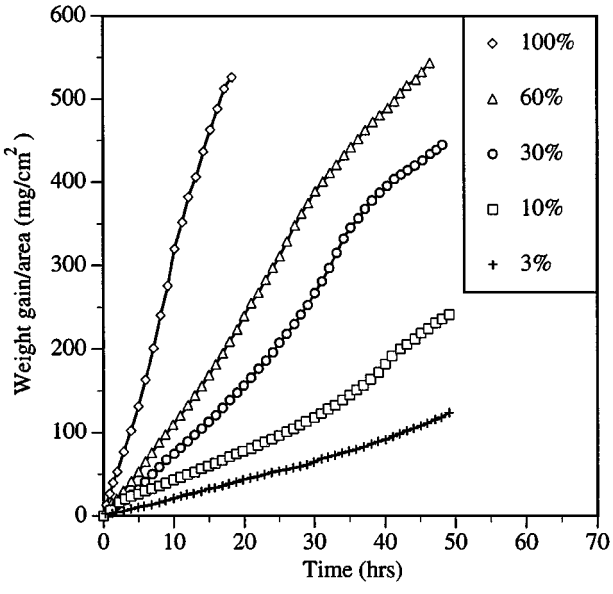

Figure 8 Weight changes for pure tin at 800 °C in various oxygen pressures.

The surface appearance of the oxidized specimens is also useful in the interpretation of the effects of oxygen pressure on the growth behavior. At lower oxygen pressures rather even and smooth oxide scales were generally obtained. It seems that oxides have better ability to form compact and more protective scales with decreasing oxygen partial pressures. This may be related to the effect of oxygen pressure on the defect structure of the SnO_2. This observation may also relate to the fact that growth stresses in the oxide have more time to become relieved through plastic flow at lower oxidation rates.

The results of wetting experiments for Sn/SnO_2 and $Sn\text{-}3Mg/SnO_2$ systems at 800 °C indicate that the contact angles (θ) are greater than 90° and the liquid metals do not wet the tin oxide ceramic. Thus, the rise of molten material along the cracks in the oxides is not likely unless external pressure is applied. Therefore, the metallic constituents observed in the reaction products

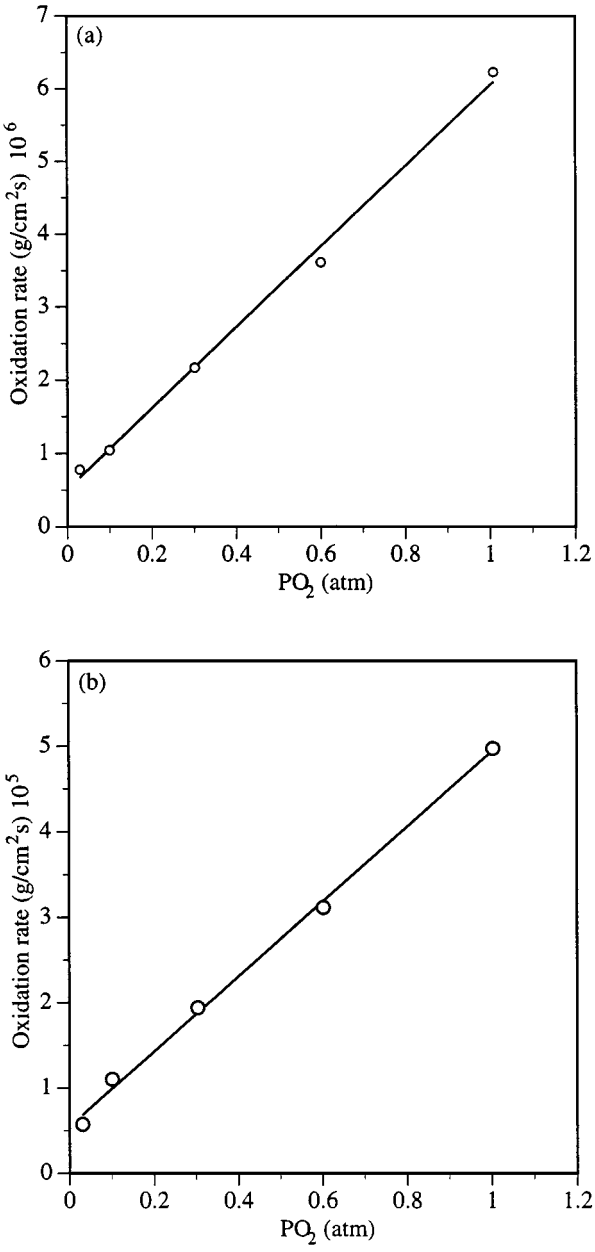

Figure 9 Rate constants for the linear oxidation of (a) tin and (b) Sn-3Mg at 800 °C as a function of oxygen pressure.

are believed to be the material left behind without being oxidized as the reaction front progresses. This is supported by the observation that the numbers of sizes of the residual metal phases tend to decrease as the reaction time is prolonged.

Several alloying additions (i.e., Ca, Mg, Ba and La) have been shown to result in a 95% increase in the oxidation rate over pure tin at 800 °C. Such a significant rate increase cannot be fully accounted for by the higher heat of oxide formation [17], due to the low concentrations used. Therefore, it becomes important to identify where are the solution elements. Since XRD analysis did not identify any addition-containing phases, TEM was then employed to further characterize the resulting oxide materials. Fig. 10 shows the [001] electron diffraction pattern of the pure SnO_2 material, where the ($hk0$) planes are absent when $h + k =$ odd. According to the extinction rule in Table III, however, there should be no restrictions on the ($hk0$) type reflections for $P4_2/mnm$, which is the space group of SnO_2. One probable explanation is the intensities of those reflections are extremely weak. This argument is supported by both the published powder X-ray diffraction data and simulated diffraction pattern of SnO_2 (Table IV), in which the ($hk0$) planes ($h + k =$ odd) are essentially non-existent. For comparison, Fig. 11a is the diffraction pattern obtained from the reaction product of Sn-3Mg alloy oxidized at 800 °C. As can be seen, superlattice reflections of the type ($h00$) (h odd) are observed. An analogous TEM diffraction pattern is shown in Fig. 11b for the oxidation product of Sn-3Ba alloy. Diffraction patterns [$\bar{1}02$] of the two oxide (Fig. 12a and b) again show superlattice reflections of the type ($h00$) (h odd) and ($h0l$) ($h + l =$ odd). The above results indicate that solute atoms (i.e., Mg and Ba) have dissolved in the SnO_2 and preferentially replaced one of the two tin atoms. TEM centered dark field images obtained by using the superlattice reflections exhibit no phase separation in the SnO_2 grains. This supports the suggestion that the origin of these superlattice reflections is solely attributed to the ordering in the structure. As a result of the ordering, some symmetry elements in the space group of pure SnO_2 are destroyed. The new MgO (BaO) doped SnO_2 materials therefore have space group P4/mmm instead of $P4_2/mnm$. Simulated X-ray diffraction data illustrate the intensity difference for those superlattice reflections with and without the dopant (Table IV).

TABLE III Extinction rules for the space group $P4_2/mnm$

Type of reflection	Reflection condition
$0kl$	$k + l = 2n$
$00l$	$l = 2n$
$h00$	$h = 2n$

TABLE IV Intensities for simulated X-ray powder diffraction pattern for pure and MgO doped SnO_2 materials

hkl	I_{SnO_2} (JCPD21-1250)	I_{SnO_2}	$I_{MgO\ doped\ SnO_2}$
100	—	—	82
110	100	100	100
001	—	—	16
101	80	88	64
200	25	22	14
111	6	4	26
210	2	0.3	20
201	—	—	14
211	65	57	62
220	18	14	16
002	8	7	8
300	—	—	4
102	—	—	6
310	14	13	11
221	—	0.1	6
112	18	13	13
301	16	14	19
311	—	0.2	8
202	8	6.5	5
320	—	—	13
212	—	0.1	6
321	12	11	7
400	4	3	3

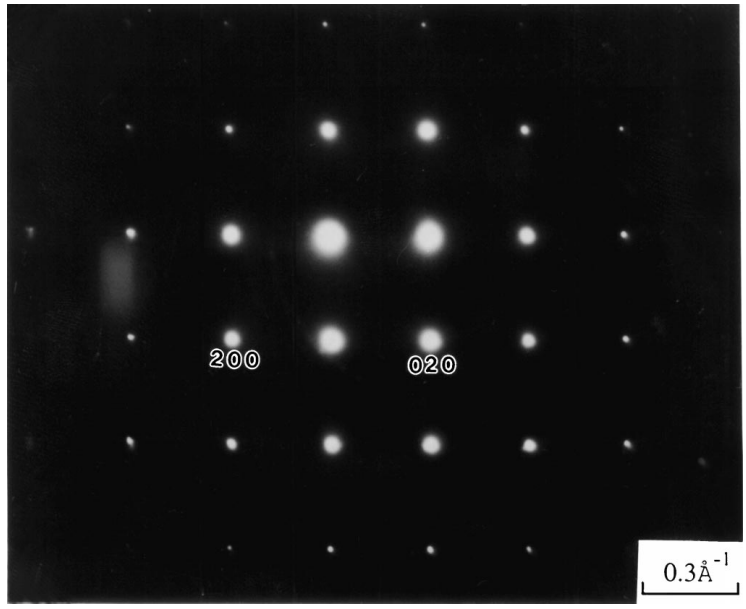

Figure 10 [001] electron diffraction patterns for pure tin oxide.

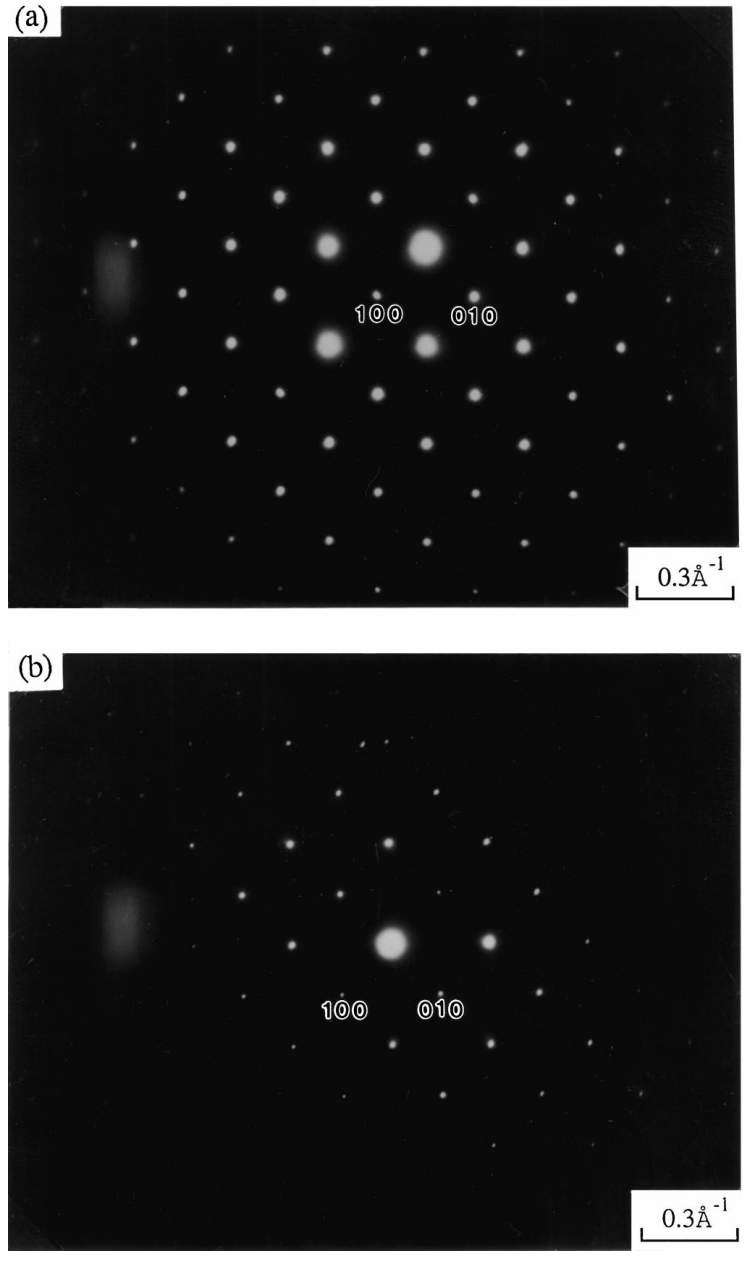

Figure 11 [001] electron diffraction patterns for (a) Sn-3Mg and (b) Sn-3Ba alloys oxidized at 800 °C in oxygen.

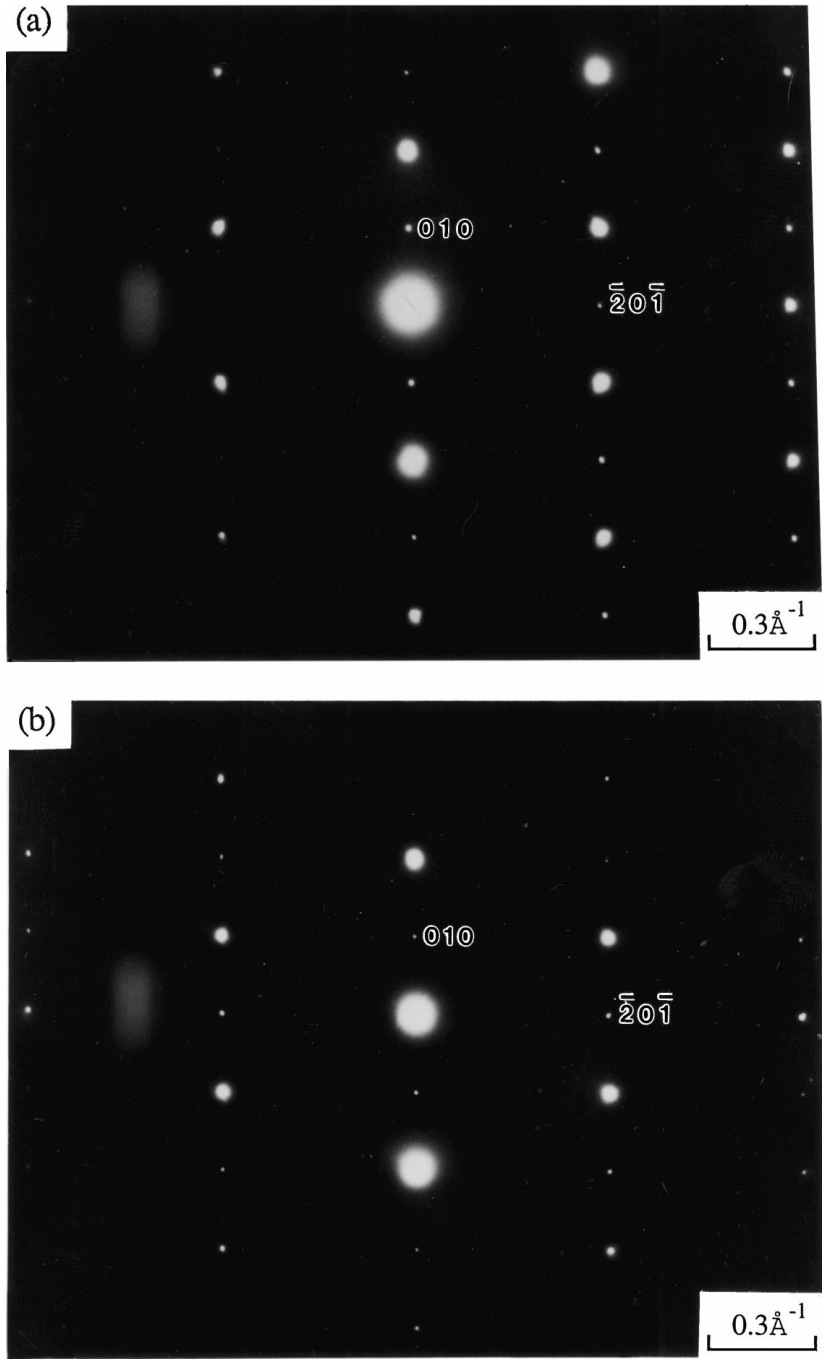

Figure 12 [$\bar{1}$02] electron diffraction patterns for (a) Sn-3Mg and (b) Sn-3Ba alloys oxidized at 800 °C in oxygen.

It is known that the linear oxidation rate is primarily associated with the formation of porous oxide scales. Such non-protective oxide provides paths for molecular oxygen that can penetrate to the scale/metal interface. Therefore, the increases in oxidation kinetics for Sn alloying with low concentrations of Mg and Ba cannot be explained by the Hauffe's valence rules, which accounts for only diffusion-controlled processes. Howes and Richardson observed that local compositional change in the growing oxide may result in the development of stresses [18]. Stringer suggested that a defect gradient in the oxide scale can also introduce growth stresses [19]. For Sn-Mg alloys, for instance, the preferentially oxidized Mg certainly introduces local heterogeneity in terms of composition and oxygen vacancy concentration into the oxide scale due to doping. As a result, the increased growth stresses make the oxide scale even less protective and more susceptible to the attack of oxygen at oxide/metal interfaces, which leads to the significant increases in the oxidation rates of the binary alloys.

4. Conclusions

Pure tin and its alloys were oxidized at temperature ranging from 600 to 800 °C in oxygen. Rapid oxidation kinetics were observed for pure liquid tin held at temperatures higher than 700 °C. The porous scale revealed in the initial stage of oxidation suggests that the reaction occurs at oxide/metal interface. The near-constant rates are attributed primarily to the phase transformation from SnO to SnO_2. In marker experiments, the

locations of Al_2O_3 markers suggest that outward diffusion of tin ions is the predominant diffusion species in the scale formation. Such observation supports the proposed oxidation mechanism that SnO, a p-type semiconductor oxide, is formed initially. In general, there is no clear-cut rate-determining process that is operative over the temperatures and oxygen pressure ranges studied.

For binary tin alloys, the alloying elements were observed to preferentially oxidize on the surface of the alloy when their oxides are thermodynamically more stable than SnO_2. The alloying additions of lower valence than stannic ion (magnesium, calcium, lanthanum and barium) increased the oxidation rate of tin. However, CaO and La_2O_3 were found to combine with SnO at 700 °C, and the rate was subsequently decreased. TEM studies showed the presence of superlattice diffraction in the oxidation products of Sn-3Mg and Sn-3Ba alloys. This clearly indicates that solute atoms (i.e., Mg and Ba) have been dissolved in the SnO_2 structure. As a result, doping of the SnO_2 scale makes it more porous by introducing additional growth stresses, and the overall oxidation rates increase.

References

1. M. S. NEWKIRK, A. W. URQUHART, H. R. ZWICKER and E. BREVAL, *J. Mater. Res.* **1** (1) (1986) 81–89.
2. M. S. NEWKIRK, H. D. LESHER, D. R. WHITE, C. R. KENNEDY, A. W. URQUHART and T. D. CLAAR, *Ceram. Eng. Sci. Proc.* **8** (1987) 879–885.
3. M. S. NEWKIRK and S. F. DIZIO, U. S. Patent no. 4,713,360 (1987).
4. K. CREBER, S. D. POSTE, M. K. AGHAJANIAN and T. D. CLAAR, *Ceram. Eng. Sci. Proc.* **9** (7/8) (1988) 975–982.
5. D.-W. YUAN, V.-S. CHENGN, R.-F. YAN and G. SIMKOVICH, *ibid.* **15** (4) (1994) 85–94.
6. D.-W. YUAN, S. G. SONG, R.-F. YAN, E. R. RYBA and G. SIMKOVICH, *J. Mater. Sci.* **34**(6) (1999) 1293–1300.
7. W. GRUHL and V. GRUHL, *Metall.* **6** (1952) 177–182.
8. G. SHIMAOKA and I. YAMAI, *J. Chem. Soc. Japan* **76** (1955) 965–967.
9. P. SPINEDI, *Gazz. Chim. ital.* **86** (1956) 579–588.
10. J. O. COPE, *Trans. Faraday Soc.* **57** (1961) 493–503.
11. D. W. ALYMORE, S. J. GREGG and W. B. JEPSON, *J. Electrochem. Soc.* **106** (1959) 1010–1013.
12. J. C. NOVER and F. D. RICHARDSON, *Trans. Inst. Min. Metall.* **81** (1972) c63–c68.
13. C. WAGNER, "Atom Movements" (ASM, Cleveland, OH, 1951).
14. T. SHUEY, "Semiconducting Ore Minerals" (Elsevier, New York, 1975).
15. W. E. BOGGS, R. H. KOCHIK and G. E. PELLISSIER, *J. Electrochem. Soc.* **110** (1963) 4–11.
16. K. HAUFFE and C. GENSCH, *Z. Physik. Chem.* **195** (1950) 116–128.
17. O. KUBASCHEWSKI, E. EVANS and C. B. ALCOCK, "Metallurgical Thermochemistry" (Pergamon Press, New York, 1967) pp. 304–363.
18. V. R. HOWES and C. N. RICHARDSON, *Corr. Sci.* **9** (1969) 385–394.
19. J. STRINGER, *ibid.* **10** (1970) 513-543.

Received 7 September 1997
and accepted 15 December 1998